Dynamics of highly supercooled liquids far from equilibrium

Ryoichi Yamamoto and Akira Onuki

Department of Physics, Kyoto University, Kyoto 606, Japan

Abstract. We first review our recent simulation work on dynamic heterogeneity and supercooled liquid rheology. We then treat a supercooled polymer melt to study the stress relaxation function, transient stress evolution, shear thinning, and elongation of chains.

(Some figures in this article appear in colour in the electronic version; see `www.iop.org`)

1. Introduction

A number of MD simulations have detected mobile clusters or strings in coexistence with immobile regions in supercooled model binary mixtures with various visualization methods [1–6]. This suggests that rearrangements of particle configurations in glassy materials are cooperative, involving many molecules. On the other hand, some experiments have shown that the diffusion constant D of a tagged particle in a supercooled liquid is considerably larger than that predicted by the Einstein–Stokes relation [7, 8]. The same tendency has been confirmed by MD simulations [9–11]. Its origin is now ascribed to coexistence of relatively active and inactive regions among which the diffusion constant varies significantly. To study these aspects numerically, we introduced *bond breakage* among adjacent particle pairs and obtained the correlation length ξ which grows up to the system size as T is lowered [4, 5]. We then studied heterogeneity in the particle diffusivity [11], which is essentially the same as that in the bond breakage.

As another direction in this field, we stress the importance of nonlinear, nonequilibrium processes such as aging effects and nonlinear rheology in supercooled liquids. We studied the latter problem and found that the externally applied shear with rate $\dot{\gamma}$ induces jump motions or bond breakage when $\dot{\gamma}$ exceeds the inverse α-relaxation time [5, 12]. Thus a strongly nonlinear regime is encountered even for extremely small $\dot{\gamma}$. Remarkably, ξ decreases with increasing $\dot{\gamma}$, so $\dot{\gamma}$ plays a role similar to that of a magnetic field in Ising systems near the critical point. This paper summarizes these results and presents preliminary results on the rheology of short-chain systems in supercooled states.

2. Dynamic heterogeneity in a binary mixture

Our 3D binary mixture is composed of two atomic species, 1 and 2, with $N_1 = N_2 = 5000$ particles in a cubic box with dimension $L = V^{1/3} = 23.2$ under periodic boundary conditions. They interact via the soft-core potentials $v_{ab}(r) = \epsilon(\sigma_{ab}/r)^{12}$ with $\sigma_{ab} = (\sigma_a + \sigma_b)/2$ $(a, b = 1, 2)$, and the mass ratio is $m_2/m_1 = 2$. The size ratio is taken at $\sigma_2/\sigma_1 = 1.2$ to prevent crystallization [2]. The particle density is fixed at $(N_1 + N_2)/V = 0.8/\sigma_1^3$. We

will measure space and time in units of σ_1 and $\tau_0 = (m_1\sigma_1^2/\epsilon)^{1/2}$. The temperature T will be measured in units of ϵ/k_B, and the viscosity η in units of $\epsilon\tau_0/\sigma_1^3$. We take long annealing times at low T to suppress aging effects. We apply shear as follows: after a long equilibration time in a quiescent state ($t < 0$), the average velocity $\dot{\gamma}y$ is added to the velocities of all the particles in the x-direction at $t = 0$. Then the shear flow is maintained by using the Lee–Edwards boundary condition [13]. In our case shear flow serves to destroy glassy structures and produces no long-range structure.

2.1. Bond breakage and structural relaxation

Owing to the sharpness of the first peak of the pair correlation functions $g_{ab}(r)$, we can unambiguously define *bonds* between particle pairs at distances close to the first peak position [4, 5]. That is, the particle pair i and j is bonded if $r_{ij}(t_0) = |r_i(t_0) - r_j(t_0)| \leqslant \ell_{1ab}$ where $i \in a$ and $j \in b$. After a lapse of time Δt, the bond is broken if $r_{ij}(t_0 + \Delta t) > \ell_{2ab}$. Here ℓ_{1ab} is longer than the distance of the first peak position of $g_{ab}(r)$, and ℓ_{2ab} ($\geqslant\ell_{1ab}$) is shorter than that of the second peak position. The number of the unbroken bonds may be fitted to $\exp[-(\Delta t/\tau_b)^c]$ as a function of the time interval Δt with $c \lesssim 1$ ($c \simeq 0.6$ at $T = 0.234$). Thus we determine the bond breakage time τ_b both in quiescent and sheared conditions. It may be fitted to a simple formula:

$$1/\tau_b(\dot{\gamma}) \cong 1/\tau_b(0) + A_b\dot{\gamma} \tag{1}$$

where A_b is a constant of order 1 in our supercooled states. For the strong-shear condition $\dot{\gamma}\tau_b(0) > 1$, we have $\tau_b(\dot{\gamma}) \sim \dot{\gamma}^{-1}$. This means that jump motions are induced by applied shear on the timescale of $\dot{\gamma}^{-1}$. At zero shear the bond breakage occurs by thermal activation and $\tau_b(0) \sim 10\tau_\alpha$, where τ_α is obtained from the decay of the self-part of the time correlation function as $F_s(q, \tau_\alpha) = e^{-1}$ at $q = 2\pi$. We define the structure factor of the broken bonds as

$$S_b(q) = \left\langle \left| \sum_{\text{broken bonds}} \exp(iq \cdot R_{ij}) \right|^2 \right\rangle \tag{2}$$

where $R_{ij} = \frac{1}{2}(r_i(t_0) + r_j(t_0))$. The summation is over the broken pairs in a time interval $[t_0, t_0 + \Delta t]$. Then, $S_b(q)$ can be fitted to the Ornstein–Zernike form:

$$S_b(q) = S_b(0)/(1 + \xi^2 q^2)$$

as shown in figure 1, where $\Delta t = 0.05\tau_b(0)$. The correlation length ξ is determined from this expression. The clusters of the broken bonds are analogous to the critical fluctuations in Ising systems. As in critical dynamics, we have furthermore confirmed a dynamical scaling relation:

$$\tau_b \sim \xi^z \tag{3}$$

where $z = 4$ in 2D and $z = 2$ in 3D. This relation holds even for strong shear $\dot{\gamma}\tau_b(0) \gg 1$, where $\xi \sim \dot{\gamma}^{-1/z}$. The shear with rate $\dot{\gamma}$ thus suppresses the heterogeneity, which is analogous to the effect of a magnetic field h on the critical fluctuations in Ising systems.

2.2. Heterogeneity in diffusion

As shown in figure 2, our simulation results for the diffusion constant of a tagged particle of the species 1 can be fitted to $D \propto \eta^{-0.75}$ at low T. On the other hand, τ_α is proportional to the viscosity η as $\tau_\alpha \sim \eta/T$. In the following we visualize the heterogeneity of the diffusivity. We pick up mobile particles of each species a (1 or 2) with the amplitude of the displacement vector $\Delta r_j(t)$ exceeding a lower limit $\ell_c(t)$ in a time interval $[t_0, t_0 + t]$. Here $\ell_c(t)$ is defined
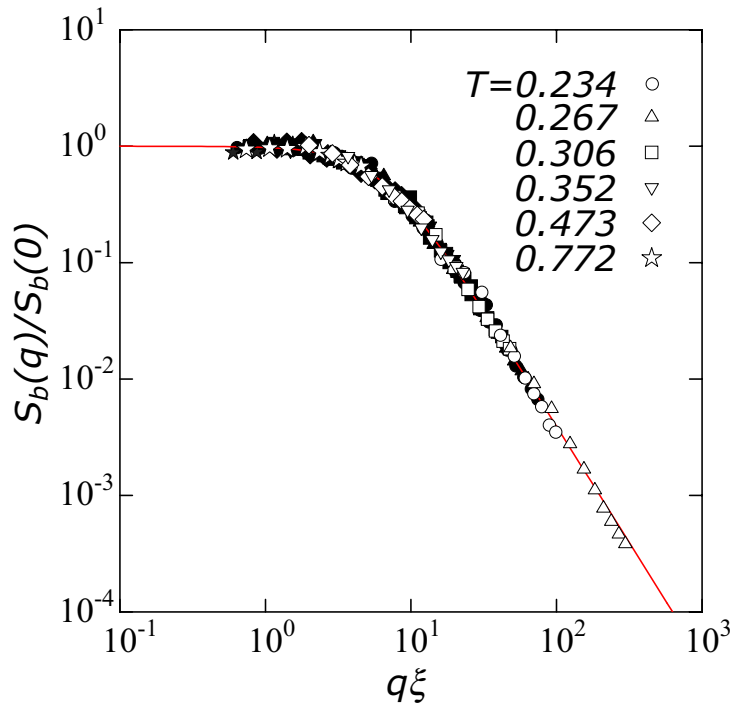
Figure 1. $S_b(q)/S_b(0)$ on logarithmic scales for various T and $\dot{\gamma}$ in 3D. Open and closed symbols represent results for $\dot{\gamma} = 0$ and $\dot{\gamma} \neq 0$, respectively. The solid line is the OZ form $1/(1 + x^2)$ with $x = q\xi$.
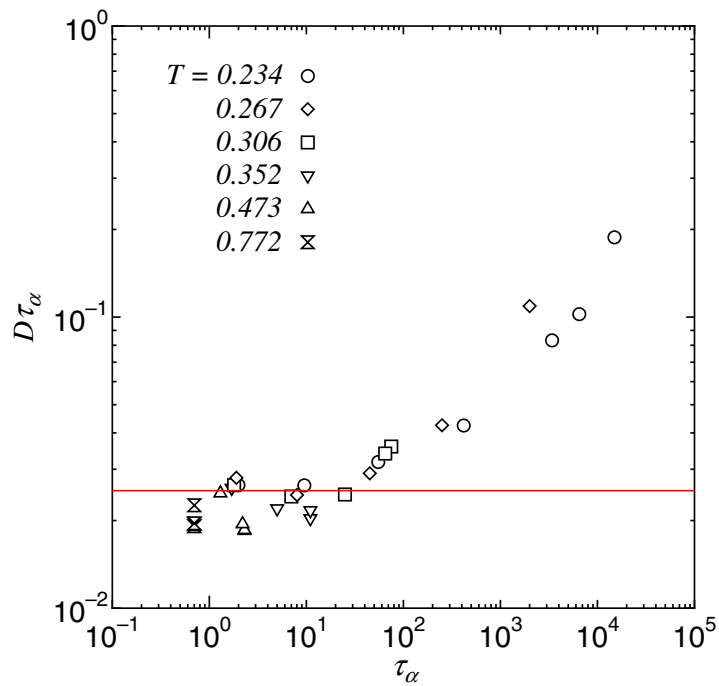

Figure 2. $D\tau_\alpha$ versus τ_α. The solid line represents the Stokes–Einstein value $D_{ES}\tau_\alpha = (2\pi)^{-2}$.
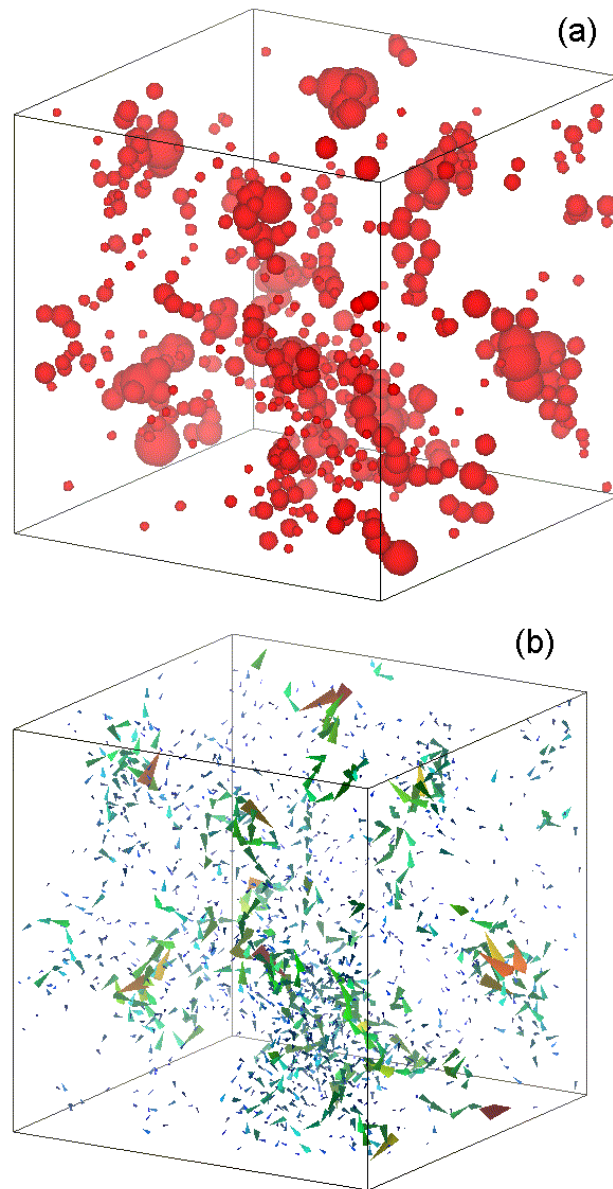
Figure 3. Mobile particles in a time interval $t = 0.125\tau_\alpha$ at $T = 0.267$. The darkness of the spheres and cones represents the depth in the 3D space. (a) Those of the smaller species 1 represented by spheres with radii $a_j(t)$ in (4). (b) Those of the species 1 and 2 represented by cones. (c) Those belonging to the clusters with sizes $n \geqslant 5$ in (b).

such that the sum of $\Delta r_j(t)^2$ for the mobile particles is 66% of the total sum ($\widetilde{=}6D_a t N_a$ for $t \gtrsim 0.1\tau_\alpha$ with $a = 1, 2$). In figure 3(a) the mobile particles of the smaller species 1 in a time interval of $[t_0, t_0 + 0.125\tau_\alpha]$ are depicted as spheres with radius

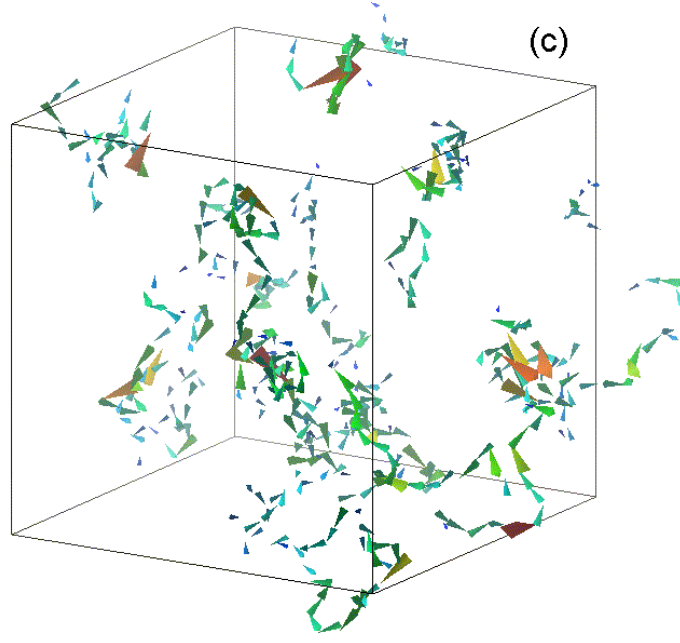$$a_j(t) = |\Delta r_j(t)| \left/ \sqrt{\left\langle \sum_{\ell \in 1} (\Delta r_\ell(t))^2 \right\rangle \middle/ N_1} \right. \tag{4}$$

Figure 3. (Continued)

located at $R_j(t) = \frac{1}{2}[r_j(t_0) + r_j(t_0 + t)]$. The chosen particles number 571. The heterogeneity is most marked for this time interval in which the non-Gaussian parameter is maximum. In figure 3(b), the displacement vectors of the mobile particles of both the species 1 and 2 are represented by cones with the base centre and the tip being the initial and final positions, respectively. We then group the mobile particles into clusters with particle number $n = 1, 2, \ldots$, where the mobile particles $i \in a$, $j \in b$ belong to the same cluster if either of $|r_i(t_0) - r_j(t_0 + t)|$ or $|r_i(t_0 + t) - r_j(t_0)|$ is shorter than $0.3(\sigma_a + \sigma_b)$. In figure 3(c) we pick up those belonging to the clusters with $n \geqslant 5$. They make up 5% of the total number of particles N, but they contribute 40% to the sum $\langle \sum_\ell (\Delta r_\ell(t))^2 \rangle$ for all the particles. The mobile particles thus form chains as reported in reference [6]. Moreover, we should note that these chains aggregate to form large-scale heterogeneities on the scale of ξ.

To examine the time evolution of the heterogeneity structure we introduce the *diffusivity density* $\sum_j a_j(t)^2 \delta(r - R_j(t))$ of the species 1 or its Fourier component:

$$\mathcal{D}_q(t_0, t) = \sum_{j \in 1} a_j(t)^2 \exp[-iq \cdot R_j(t)]. \tag{5}$$

Here the immobile particles are nearly negligible in the summation due to the weight $a_j(t)^2$. In the particle displacements, t_0 is the initial time and $t_0 + t$ is the final time, so t is the time interval. The structure factor $S_D(q, t) = \langle |\mathcal{D}_q(t_0, t)|^2 \rangle$ behaves very similarly to the broken-bond structure factor (2) with the same correlation length ξ. By displacing the initial time t_0 to $t_0 + \tau$ with the time interval t fixed, we may introduce the time correlation function:

$$S_{\mathcal{D}}(q, t, \tau) = \langle \mathcal{D}_q(t_0 + \tau, t)\mathcal{D}_{-q}(t_0, t) \rangle \tag{6}$$

which is obtained after averaging over many initial states. Then $S_{\mathcal{D}}(q, t, 0) = S_{\mathcal{D}}(q, t)$. In figure 4 we show the relaxation of $S_{\mathcal{D}}(q, \tau_\alpha, \tau)/S_{\mathcal{D}}(q, \tau_\alpha, 0)$ as a function of τ for three q. It may be fitted to $\exp[-(\tau/\tau_h(q))^c]$ with $c = 0.5$. The relaxation time $\tau_h(q)$ is about $3\tau_\alpha$
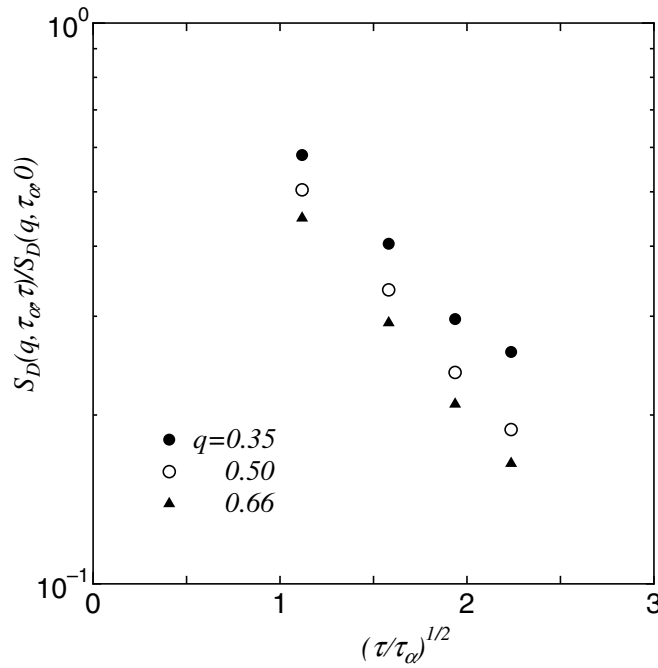
Figure 4. $S_{\mathcal{D}}(q, \tau_\alpha, \tau)/S_{\mathcal{D}}(q, \tau_\alpha, 0)$ versus $(\tau/\tau_\alpha)^{1/2}$ for $q = 0.35, 0.5,$ and 0.66. This represents the decay of the heterogeneity structure.

at $T = 0.267$ and $q = 0.35$ (which is the smallest wavenumber, $2\pi/L$). It decreases with decreasing q and saturates for $q \lesssim \xi^{-1}$. The two-time correlation function for the broken-bond density also relaxes with $\tau_h(q)$ in the same manner.

3. Rheology in a supercooled binary mixture

In our fluid mixtures in supercooled states, non-Newtonian behaviour appears for $\dot\gamma$ larger than $\tau_b(0)^{-1} \sim 0.1\tau_\alpha^{-1}$. We demonstrated that the steady-state viscosity $\eta(\dot\gamma) = \sigma_{xy}/\dot\gamma$ is determined by the bond breakage time in (1) as

$$\eta(\dot\gamma) \cong A_\eta \tau_b(\dot\gamma) + \eta_B \tag{7}$$

where A_η and η_B are constants of order 1 for our supercooled states. This form agrees with an experiment by Simmons *et al* [14]. In particular, $\eta(\dot\gamma) \cong (A_\eta/A_b)/\dot\gamma + \eta_B$, for $\dot\gamma\tau_b(0) \gg 1$, using (1). If the background η_B is negligible, a constant limiting stress follows as $\sigma_{xy} = A_\eta/A_b$. The physical mechanism of this behaviour is as follows [5]. Upon each bond breakage induced by shear, the particles involved release a potential energy of order ϵ. It is then changed into energies of random motions supported by the surrounding particles. The heat production rate is estimated as $Q \sim n\epsilon/\tau_b(\dot\gamma) \sim n\epsilon\dot\gamma$, where n is the number density. Because Q is related to the viscosity by $Q = \sigma_{xy}\dot\gamma$, we obtain $\sigma_{xy} \sim n\epsilon$ for high shear. Interestingly, similar *jamming dynamics* has begun to be recognized also in the rheology of foams [15–17] and granular materials [18] composed of large elements. Shear-thinning behaviour and heterogeneities in configuration rearrangements are commonly observed also in these macroscopic systems.

4. Rheology in a supercooled polymer melt

Recent simulations on glassy polymer melts have mainly treated self-motions of particles in quiescent states [19–21]. We will study the rheological properties of glassy polymers, for which not enough theoretical effort has been made. In our model all the bead particles interact with a Lennard-Jones potential of the form [19, 21]

$$U_{LJ}(r) = 4\epsilon[(\sigma/r)^{12} - (\sigma/r)^6] + \epsilon.$$

It is cut off at the minimum distance $2^{1/6}\sigma$, so we use its repulsive part only to prevent spatial overlap of particles. Consecutive beads on each chain are connected by an anharmonic spring of the form

$$U_F(r) = -\frac{1}{2}k_c R_0^2 \ln[1 - (r/R_0)^2]$$

with $k_c = 30\epsilon/\sigma^2$ and $R_0 = 1.5\sigma$. In a cubic box with length $L = 10\sigma$ under periodic boundary conditions, we put $M = 100$ chains composed of $N = 10$ beads. The number density is fixed at $n = NM/V = 1/\sigma^3$. The bond lengths $b_j = |R_j - R_{j+1}|$ between consecutive beads on each chain are nearly fixed at the minimum $b_0 \cong 0.96$ of $U_{LJ}(r) + U_F(r)$. We will measure space, time, and T in units of σ, $\tau_0 = (m\sigma^2/\epsilon)^{1/2}$, and ϵ/k_B where m is the bead mass.

As in references [19–21], we confirmed that the relaxation time of the pth mode of a chain is well described by the Rouse result:

$$\tau_p = \zeta b^2/[12T \sin^2(p\pi/2N)] \qquad (1 \leqslant p \leqslant N - 1)$$

in quiescent supercooled states. Here the end-to-end vector of a chain $P = R_N - R_1$ has the variance $\langle P^2 \rangle = (N - 1)b^2$, and obeys a Rouse relaxation, yielding the statistical segment length b ($\cong 1.2$) and the friction constant ζ. The Rouse time τ_R ($=\tau_1$) then increases drastically with lowering T as $\tau_R = 250$, 1800, and 6×10^4 for $T = 1.0$, 0.4, 0.2, respectively. We also calculated the α-relaxation time τ_α using the self-correlation function as $F_q(\tau_\alpha) = e^{-1}$ at $q = 2\pi$ [31]. Then we obtained $\tau_R \cong 2N^2\tau_\alpha$ for our system.

4.1. Stress relaxation in the linear regime

Now let us discuss the linear viscoelastic behaviour in supercooled states [22]. In figure 5 we show the stress relaxation function

$$G(t) = \langle \sigma_{xy}^T(t)\sigma_{xy}^T(0)\rangle/VT \tag{8}$$

where σ_{xy}^T is the space integral of the xy-component of the total stress tensor over the volume $V = L^3$. At the lowest temperature $T = 0.2$, $G(t)$ exhibits salient features of glassy polymer melts [22]. From the initial value of order 100, $G(t)$ relaxes to a value G_0 of about 5 for $t \gtrsim 1$. We then have a slow decay of the KWW form:

$$G(t) \cong G_0 \exp[-(t/\tau_s)^\beta] \tag{9}$$

in the region $1 \lesssim t \lesssim 10\tau_s$, where $\tau_s = 90 \sim \tau_\alpha$ and $\beta = 0.5$. This glassy behaviour arises from monomeric structural relaxation [22]. For $t \gtrsim 50\tau_s$ it approaches the Rouse stress relaxation function:

$$G_R(t) = nTN^{-1} \sum_{1 \leqslant p \leqslant N-1} \exp(-2t/\tau_p) \tag{10}$$

which decays as $nTN^{-1} \exp(-2t/\tau_R)$ for $t \gg \tau_R$. This final-stage behaviour arises from relaxation of large-scale chain conformations. Experimentally, however, the intermediate
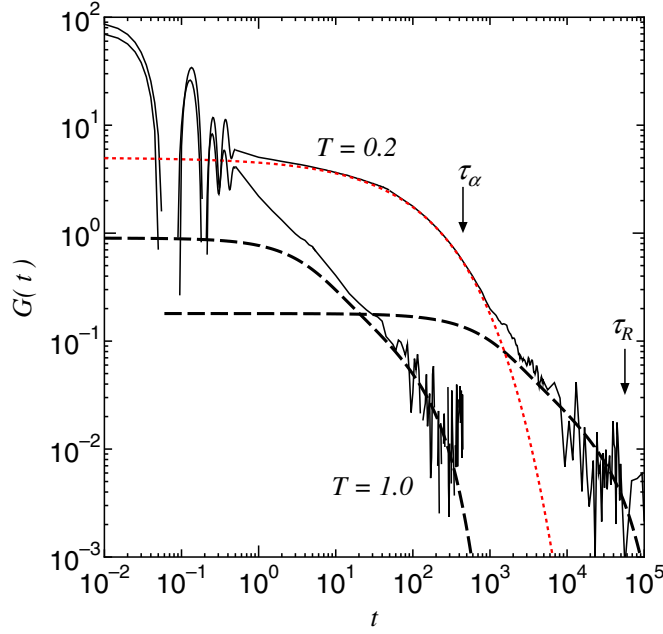
Figure 5. The stress relaxation function $G(t)$ (thin solid lines) at $T = 0.2$ in a supercooled state and $T = 1$ in a normal-liquid state. It may be fitted to the stretched-exponential form (dotted line) at relatively short times and tends to the Rouse relaxation function $G_R(t)$ (bold dashed lines) at long times.

region, which connects the glassy and polymeric (Rouse or reptation) relaxations, extends over a much wider time range (typically four decades [22]), and $G(t)$ there has been fitted to an algebraic form, $G(t) \cong e^{-1} G_0(t/\tau_s)^{-a}$ with $a \sim 0.5$ [22]. In addition, on increasing the molecular weight, a rubbery plateau has been observed to develop after the crossover before the terminal decay, whereas it is apparently not seen for our short-chain system. The zero-frequency linear viscosity η consists of a monomeric part $\Delta \eta$ of order $10\tau_s$ from the integration in the time region $t \lesssim 10\tau_s$ and the Rouse viscosity

$$\eta_R = \int_0^\infty dt \, G_R(t) \cong 0.808 T N^{-1} \tau_R$$

from $t \gtrsim \tau_R$. The ratio $\Delta \eta / \eta_R$ is thus of order $1/TN$ (~ 1 for $T = 0.2$ and $N = 10$), whereas we should have $\Delta \eta \ll \eta_R$ for much larger N.

In the Rouse model, the total polymer (entropic) stress $\sigma_{\alpha\beta}^R$ is the sum of $T b_{j\alpha} b_{j\beta} / b^2$ over all of the bonds in the system, where the $b_{j\alpha}$ are the components of the bond vectors $\boldsymbol{b}_j = \boldsymbol{R}_{j+1} - \boldsymbol{R}_j$. We confirmed that the relaxation function $G_c(t) = \langle \sigma_{xy}^R(t) \sigma_{xy}^R(0) \rangle / VT$ nearly coincides with $G_R(t) \cong G(t)$ for $t \gtrsim 0.1\tau_R$, whereas it is about half of $G_R(t)$ for $t \lesssim \tau_s$. The bond orientation tensor $Q_{\alpha\beta}$ may be defined as

$$Q_{\alpha\beta} = \sum_{1 \leqslant j \leqslant N-1} \langle b_{j\alpha} b_{j\beta} \rangle / b^2 (N-1) \qquad (\propto \langle \sigma_{\alpha\beta}^R \rangle).$$

If the polarizability tensor of a bead is uniaxial along the bond vector, the deviation of the dielectric tensor $\Delta \varepsilon_{\alpha\beta}$ is proportional to $Q_{\alpha\beta} - \delta_{\alpha\beta}/3$. For flow birefringence we have $\Delta \varepsilon_{xy} = C \langle \sigma_{xy}^R \rangle / V$, where C is a constant. In supercooled states, $\langle \sigma_{xy}^R \rangle / V$ can be much smaller than the total shear stress σ_{xy}—for instance, in transient states or for oscillatory shear. The usual stress–optical law $\Delta \varepsilon_{xy} = C \sigma_{xy}$ valid far above T_g breaks down close to T_g [23–26].

4.2. Nonlinear shear effects

In figure 6 we show the stress growth function $\sigma_{xy}(t)/\dot{\gamma}$ after application of shear at $t = 0$ at $T = 0.2$ for various $\dot{\gamma}$. In the initial stage, in which $\dot{\gamma}t \lesssim 0.1$, we can see the linear viscoelastic growth, $\sigma_{xy}(t)/\dot{\gamma} = \int_0^t G(t') \, dt'$, whereas a nonlinear regime sets in for $\dot{\gamma}t \gtrsim 0.1$, resulting in the non-Newtonian viscosity $\eta(\dot{\gamma})$. As a guide, we also plot the linear growth function $\int_0^t G_R(t') \, dt'$ from the Rouse model, which is far below the true linear growth for $t \ll \tau_R$. The relevant physical processes are as follows: for $\dot{\gamma}t \lesssim 0.1$ the overall chain conformations are affinely deformed, whereas for $\dot{\gamma}t \gtrsim 0.1$ the structural rearrangements among beads belonging to different chains become appreciably induced by shear. Experimentally, however, a stress overshoot has been observed at $\dot{\gamma}t = 0.05$–0.1 for higher-molecular-weight melts close to T_g [22]. In figure 7 we display the steady-state viscosity $\eta(\dot{\gamma})$. It exhibits marked shear-thinning behaviour for $\dot{\gamma}\tau_R \gtrsim 1$ and becomes independent of T for very high shear rates. The horizontal arrows indicate the linear Rouse viscosity η_R, and the vertical arrows indicate the points at which $\dot{\gamma} = \tau_R^{-1}$. In particular, the curve for $T = 0.2$ may be fitted to $\eta \propto \dot{\gamma}^{-\nu}$ with $\nu \simeq 0.7$ for $\dot{\gamma}\tau_R \gtrsim 1$. Similar shear thinning has been reported in MD simulations of short-chain systems in normal-liquid states, but at much higher shear rates [25, 27, 28].
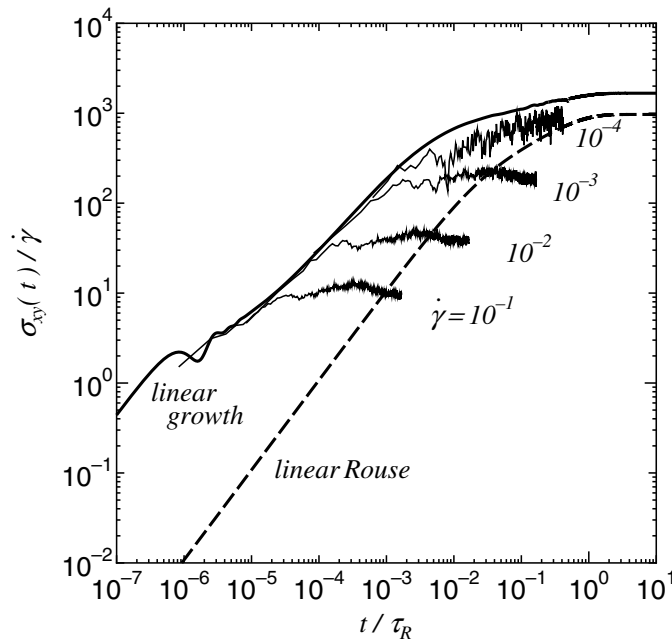

Figure 6. Shear stress divided by shear rate $\dot{\gamma} = 10^{-1}, 10^{-2}, 10^{-3}, 10^{-4}$ (thin solid lines) versus t/τ_R (where $\tau_R = 6 \times 10^4$) at $T = 0.2$. The curves follow the linear growth function (bold solid line) for $\dot{\gamma}t \lesssim 0.1$, but afterwards depart from it. The linear growth function in the Rouse model is also plotted (bold dashed line).

We next examine the anisotropy in the chain conformations under shear at $T = 0.2$ and $\dot{\gamma} = 10^{-4}$. In figure 8(a), we plot the x–y cross section ($z = 0$) of the steady-state bead distribution function:

$$g_s(\boldsymbol{r}) = \sum_{1 \leqslant j \leqslant N} \langle \delta(\boldsymbol{R}_j - \boldsymbol{R}_G - \boldsymbol{r}) \rangle / N \tag{11}$$

where $\boldsymbol{R}_G(t) = N^{-1} \sum_{n=1}^N \boldsymbol{R}_n(t)$ is the centre of mass of a chain. In figure 8(b), we plot the
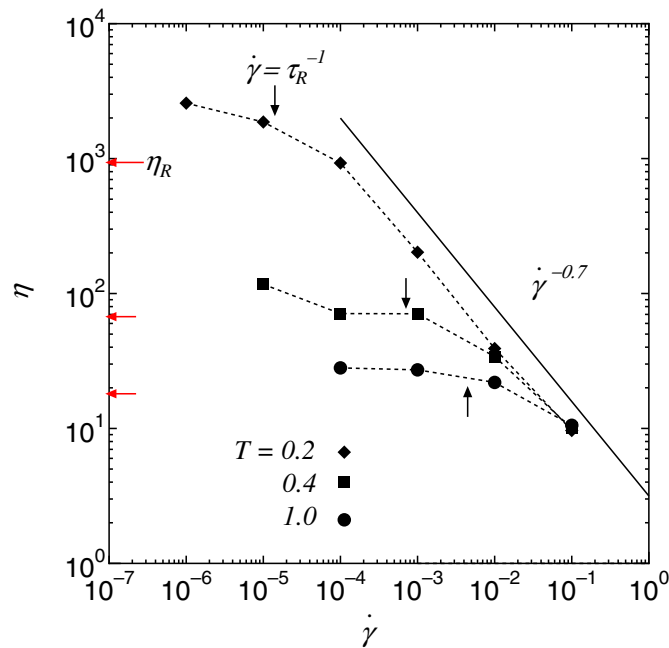
Figure 7. The steady-state viscosity versus $\dot{\gamma}$ for $T = 0.2$, 0.4, 1. A line of slope -0.7 is also given as a guide to the eye.
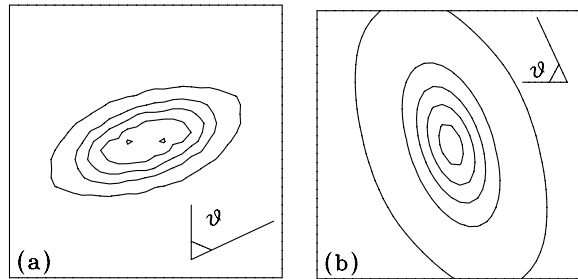

Figure 8. (a) Isointensity curves of $g_s(\boldsymbol{r})$ in equation (9) in the xy-plane ($-3.75 < x, y < 3.75$, $z = 0$). (b) Those of the incoherent structure factor $S(\boldsymbol{q})$ in equation (10) in the $q_x q_y$-plane ($-\pi < q_x, q_y < \pi$, $q_z = 0$). The values for the isolines are $0.01 + 0.02n$ in (a) and $0.1 + 0.2n$ in (b) with $n = 0, 1, \ldots, 4$ from outer to inner line. Here $T = 0.2$, $\dot{\gamma} = 10^{-4}$, and the flow is in the horizontal (x-) direction. θ is the angle between the average chain shapes and the y-axis.

structure factor:

$$S(\boldsymbol{q}) = \sum_{1 \leqslant i, j \leqslant N} \langle \exp(\mathrm{i}\boldsymbol{q} \cdot (\boldsymbol{R}_i - \boldsymbol{R}_j)) \rangle / N^2 \tag{12}$$

in the $q_x q_y$-plane ($q_z = 0$). It is proportional to the intensity of the scattering from labelled chains under shear [29]. We recognize that $g_s(\boldsymbol{r})$ and $S(\boldsymbol{q})$ almost saturate into the forms shown in figure 8 for $\dot{\gamma} \gtrsim 10/\tau_R$. The figures indicate that our short chains take ellipsoidal shapes on average once $\dot{\gamma} \gtrsim 10/\tau_R$. Let us define the tensor

$$I_{\alpha\beta} = \sum_{1 \leqslant i, j \leqslant N} \langle (\boldsymbol{R}_i - \boldsymbol{R}_j)_\alpha (\boldsymbol{R}_i - \boldsymbol{R}_j)_\beta \rangle / N^2.$$

For small q with $q_z = 0$, we have the expansion

$$S(q) = 1 - \frac{1}{2}a_1^2(q \cdot e_1)^2 - \frac{1}{2}a_2^2(q \cdot e_2)^2 + \cdots$$

where $\{e_1, e_2\}$ and $\{a_1^2, a_2^2\}$ are the unit eigenvectors and values of the tensor $I_{\alpha\beta}$ with $\alpha, \beta = x, y$. The two lengths a_1 and a_2 are the shorter and longer radii of the ellipses. In figure 9 we show $\tan\theta = -e_{1y}/e_{1x}$, the degree of elongation $1 - a_1/a_2$, and the xy-component of the orientation tensor Q_{xy}. For $\dot{\gamma}\tau_R \gtrsim 10$ we have $\theta \cong 80°$, $a_1/a_2 \cong 0.3$, $Q_{xy} \cong 0.1$. These quantities represent the average chain forms and bond orientation, and are insensitive to T if plotted versus $\dot{\gamma}\tau_R$. We stress that the shape changes of chains start to occur at $\dot{\gamma} \sim \tau_R^{-1}$ while the monomeric structural relaxation is only slightly affected by shear. In fact, we found that the cage breakage time $\tau_b(\dot{\gamma})$ for neighbouring beads belonging to different chains and the shear-dependent α-relaxation time $\tau_\alpha(\dot{\gamma})$ do not change appreciably for $\dot{\gamma} \sim \tau_R^{-1}$ at $T = 0.2$. This tendency should be more evident for longer-chain systems.
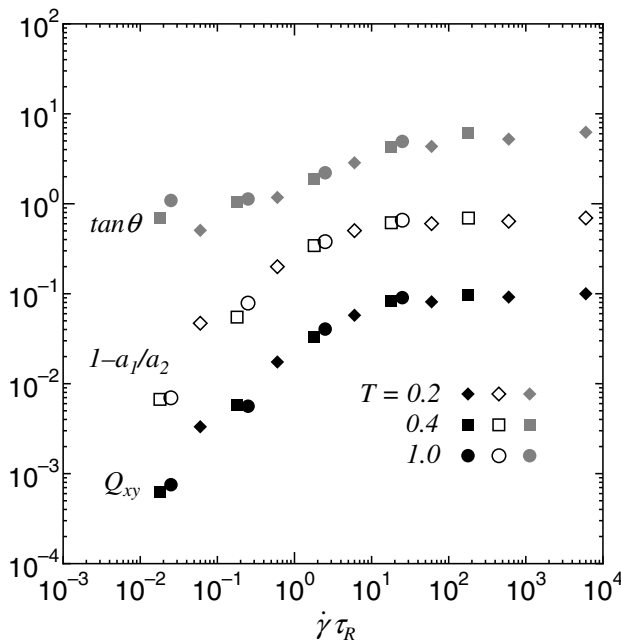

Figure 9. $\tan\theta$, $1 - a_1/a_2$, and Q_{xy} versus $\dot{\gamma}\tau_R$.

5. Concluding remarks

We have presented some examples of far-from-equilibrium problems for glassy materials. In particular, a marked analogy with critical phenomena has been pointed out for a binary fluid mixture. However, the true meaning of the correlation length ξ of the heterogeneity remains not clear. We need to understand how the dynamical quantities depend on ξ, as in the case of critical dynamics. We should also fully investigate the space-time evolution of the dynamic heterogeneity, which should influence transient relaxations, for instance, after a temperature change or application of strain. In polymer melts also, dynamic heterogeneities are enhanced at low T by the bond breakage and the monomer diffusivity [30,31]. However, they affect the centre-of-mass motions of chains little, because their characteristic lifetime is much shorter than τ_R ($\sim N^2\tau_\alpha$) for $N \gg 1$.

References

[1] Maeda K and Takeuchi S 1981 *Phil. Mag.* A **44** 643
[2] Muranaka T and Hiwatari Y 1995 *Phys. Rev.* E **51** R2735
    Muranaka T and Hiwatari Y 1997 *Prog. Theor. Phys. Suppl.* **126** 403
[3] Hurley M M and Harrowell P 1995 *Phys. Rev.* E **52** 1694
    Perera D N and Harrowell P 1996 *Phys. Rev.* E **54** 1652
[4] Yamamoto R and Onuki A 1997 *J. Phys. Soc. Japan* **66** 2545
[5] Yamamoto R and Onuki A 1998 *Phys. Rev.* E **58** 3515
[6] Kob W, Donati C, Plimton S J, Poole P H and Glotzer S C 1997 *Phys. Rev. Lett.* **79** 2827
    Donati C, Douglas J F, Kob W, Plimton S J, Poole P H and Glotzer S C 1998 *Phys. Rev. Lett.* **80** 2338
[7] Chang I, Fujara F, Geil B, Heuberger G, Mangel T and Silescu H 1994 *J. Non-Cryst. Solids* **172–174** 248
[8] Cicerone M T and Ediger M D 1996 *J. Chem. Phys.* **104** 7210
[9] Thirumalai D and Mountain R D 1993 *Phys. Rev.* E **47** 479
[10] Perera D and Harrowell P 1998 *Phys. Rev. Lett.* **81** 120
[11] Yamamoto R and Onuki A 1998 *Phys. Rev. Lett.* **81** 4915
[12] Yamamoto R and Onuki A 1997 *Europhys. Lett.* **40** 61
    Onuki A and Yamamoto R 1998 *J. Non-Cryst. Solids* **235–237** 34
[13] Evans D J and Morriss G P 1990 *Statistical Mechanics of Nonequilibrium Liquids* (New York: Academic)
[14] Simmons J H, Ochoa R, Simmons K D and Mills J J 1988 *J. Non-Cryst. Solids* **105** 313
[15] Okuzono T and Kawasaki K 1995 *Phys. Rev.* E **51** 1246
[16] Durian D J 1997 *Phys. Rev.* E **55** 1739
[17] Langer S A and Liu A J 1997 *J. Phys. Chem.* B **101** 8667
[18] Miller B, O'Hern C and Behringer R P 1996 *Phys. Rev. Lett.* **77** 3110
[19] Bennemann C, Paul W, Binder K and Dünweg B 1998 *Phys. Rev.* E **57** 843
[20] Okun K, Wolfgardt M, Baschnagel J and Binder K 1997 *Macromolecules* **30** 3075
[21] Bennemann C, Baschnagel J, Paul W and Binder K 1999 *Comput. Theor. Polym. Sci.* **9** 217
[22] Matsuoka S 1992 *Relaxation Phenomena in Polymers* (New York: Oxford)
[23] Muller R and Pesce J J 1994 *Polymer* **35** 734
[24] Kröger M, Luap C and Muller R 1997 *Macromolecules* **30** 526
[25] Kröger M, Loose W and Hess S 1993 *J. Rheol.* **37** 1057
[26] Inoue T, Ryu D S and Osaki K 1998 *Macromolecules* **31** 6977
    Matsuyama M, Watanabe H, Inoue T and Osaki K 1998 *Macromolecules* **31** 7973
[27] Chynoweth S and Michopoulos Y 1994 *Mol. Phys.* **81** 133
[28] Khare R and de Pablo J 1997 *J. Chem. Phys.* **107** 6956
[29] Muller R, Pesce J J and Picot C 1993 *Macromolecules* **26** 4356
[30] Bennemann C, Donati C, Baschnagel J and Glotzer S C 1999 *Nature* **399** 246
[31] Yamamoto R and Onuki A 2000 to be published